Sublattice Interference as the Origin of σ Band Kinks in Graphene

Sung Won Jung, Woo Jong Shin, Jimin Kim, Luca Moreschini, Han Woong Yeom, Eli Rotenberg, Aaron Bostwick, and Keun Su Kim

Sublattice Interference as the Origin of σ Band Kinks in Graphene

Sung Won Jung,[1,2] Woo Jong Shin,[1,2] Jimin Kim,[1,2] Luca Moreschini,[1,3] Han Woong Yeom,[1,2] Eli Rotenberg,[3] Aaron Bostwick,[3] and Keun Su Kim[1,2,*]

[1]*Center for Artificial Low Dimensional Electronic Systems,*
Institute for Basic Science, Pohang 37673, Korea
[2]*Department of Physics, Pohang University of*
Science and Technology, Pohang 37673, Korea
[3]*Advanced Light Source, E. O. Lawrence Berkeley*
National Laboratory, Berkeley, CA 94720, USA

Abstract

Kinks near the Fermi level observed in angle-resolved photoemission spectroscopy (ARPES) have been widely accepted to represent electronic coupling to collective excitations, but kinks at higher energies have eluded a unified description. We identify the mechanism leading to such kink features by means of ARPES and tight-binding band calculations on σ bands of graphene, where anomalous kinks at energies as high as $\sim$4 eV were reported recently [Phys. Rev. Lett. **111,** 216806 (2013)]. We found that two σ bands show a strong intensity modulation with abruptly vanishing intensity near the kink features, which is due to sublattice interference. The interference induced local singularity in the matrix element is a critical factor that gives rise to apparent kink features, as confirmed by our spectral simulations without involving any coupling to collective excitations.

Angle-resolved photoemission spectroscopy (ARPES) is an essential technique that can directly measure the electronic band structure of solids [1]. It is also useful in the study of electronic coupling to collective excitations, such as phonons and magnons, which appears as an abrupt change in the slope of band dispersion, termed "kink structure" [2–8]. So far, the low-energy kink structure observed in ARPES has been widely accepted to represent coupling to collective excitations, providing important information on their energy scale and coupling strength. However, kinks that appear at energies much higher than excitations have remained controversial, and their mechanism was hotly debated in terms of manybody interactions and spectral modulations [9–16].

The kink structure is also a central issue in the study of graphene [17–20]. Graphene has simple lattice and electronic structures, and its energy scale of phonons is relatively high [21–25], making it ideal for investigating the kink phenomenology of a two-dimensional solid. Indeed, ARPES spectra of graphene π bands show pronounced kinks in the energy scale of 140–150 meV from the Fermi energy (E_F) [17–20], which is typical of optical phonons in graphene [21].

Recently, Mazzola *et al.* have reported that ARPES spectra of graphene σ bands, having binding energies greater than 3.5 eV, show the similar kink features [26]. This is rather surprising, given that ARPES kinks typically occur within few hundred millielectronvolts from E_F and are therefore not expected at such a high binding energy. The observed kinks were attributed to electron-phonon coupling, where an abrupt drop in the density of states at the low-energy edge of σ bands is assumed to substitute for the role of the Fermi cutoff at E_F [26]. However, the estimated electron-phonon coupling strength is $\sim$1.0, which is an order of magnitude greater than in theoretical predictions for doped π bands [21–25].

In this Letter, we identify the mechanism of high-energy kinks in graphene σ bands by means of ARPES and tight-binding band calculations. We find that two σ bands show unexpectedly strong intensity modulations and abruptly vanishing intensity near the kink features. Such characteristic intensity patterns are found due to quantum interference of wavefunctions coming from two sublattices within the honeycomb lattice of graphene. The interference induced local singularity in the matrix element is identified as a key factor that leads to apparent kink features, as confirmed by our spectral simulations without involving any coupling to collective excitations. This mechanism, which is demonstrated for graphene as a simple model system, may be extended to those observed in various other materials sys-
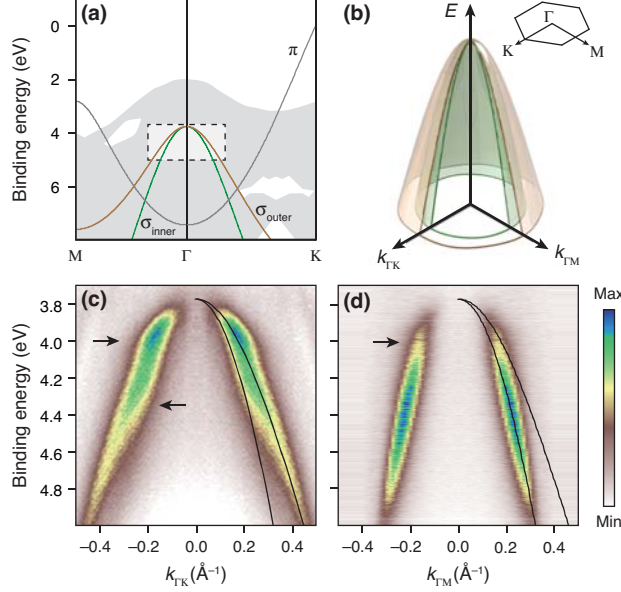
FIG. 1: (color online). (a) Valence band structure of graphene along $k_{\Gamma M}$ and $k_{\Gamma K}$ directions, obtained from the tight-binding band calculations [30]. The shaded area represents projected substrate bands [31]. (b) 3D representation of two σ bands for the boxed area in (a). The inset shows the Brillouin zone. Experimental ARPES spectra of σ bands, taken at 15 K along (c) $k_{\Gamma K}$ and (d) $k_{\Gamma M}$ directions. Black curves overlaid are a fit with calculated dispersions based on the tight-binding model. The high-energy kink features are indicated by arrows.

tems, where the similar intensity suppression near high-energy kink features was commonly observed [9–16].

ARPES experiments were performed at Beamline 4.0.3 in the Advanced Light Source, equipped with a R8000 analyzer (VG-Scienta, Sweden). Energy and momentum (k) resolutions were better than 20 meV and 0.01 Å^{-1}. The photon energy of 30–45 eV was chosen to have a good cross-section of graphene σ bands. Our sample is quasi-freestanding graphene fabricated on the surface of hydrogen-terminated 6H-SiC(0001) wafers with a dopant concentration of 1×10^{18} cm^{-3}. The graphene layer was grown *ex-situ* by thermal graphitization of SiC(0001) in a flow of argon [27], followed by annealing at 850°C in a flow of hydrogen, as described in [28, 29]. The samples were then transferred to the ultrahigh vacuum chamber with base pressure of 5×10^{-11} torr, and briefly annealed up to 500°C before ARPES measurements. For graphene on bufferlayer samples, we obtained essentially the same results in terms of σ-band kinks, which is consistent with previous results [26].

Figure 1(a) shows a wide scale valence band structure of graphene, calculated by the tight binding model [30], along ΓK and ΓM directions [Brillouin zone in Fig. 1(b)]. Near E_F, the well known π band of p_z orbitals (gray line) is linearly dispersing around the K point [17]. At binding energies greater than 3.5 eV, there are two parabolic σ bands (green and brown lines), coming from two of three bonding states of in-plane sp^2 orbitals. Near their vertex [the boxed region in Fig. 1(a)], inner and outer σ bands are closely spaced with nearly isotropic energy contours and degenerate at the Γ point, as illustrated in Fig. 1(b).

An important deviation from this simple tight-binding picture is observed in ARPES spectra taken for the corresponding k region [Figs. 1(c) and 1(d)]. Consistent with the previous report [26], there are apparent kink features, as indicated by arrows. Near these features, the spectral intensity is not uniform but strongly suppressed in $|k| < 0.1$ Å^{-1}. Because of this suppression, it is difficult to directly quantify the kink energy (E_{kink}), defined by the energy scale of kinks with respect to the top of σ bands [26]. We have optimized tight-binding parameters to reproduce the observed dispersions in $|k| \geq 0.1$ Å^{-1}, as shown by black curves overlaid in Figs. 1(c) and 1(d). The best fit yields $E_{kink} \sim 230$ meV, which is similar to but clearly greater than the typical energy scale of optical phonons in graphene [17, 18, 21]. Furthermore, we found only the outer branch (σ_{outer}) of two σ bands is visible along $k_{ΓK}$ [Fig. 1(c)], whereas only the other inner branch (σ_{inner}) is visible along $k_{ΓM}$ [Fig. 1(d)]. This is at variance with Fig. 1 of the previous report [26], where only the σ_{outer} is visible in both $k_{ΓK}$ and $k_{ΓM}$ directions. The kink features with strong intensity modulations were consistently observed with the photon energy of 30–45 eV [32] and on different substrates [26]. This rules out possible effects of final-state conditions as well as coupling to substrate bands [shaded area in Fig. 1(a)] [33].

The intensity modulation can more clearly be identified in a series of constant-energy maps in Fig. 2. From tight-binding band calculations, one would expect two nearly circular contours of σ_{outer} and σ_{inner} bands, as shown in Figs. 2(a)–2(c). Corresponding ARPES spectra are, however, strongly modulated to have a characteristic intensity pattern with sixfold symmetry [Figs. 2(d)–2(f)]. Comparing to tight-binding band contours (black lines overlaid), we found that σ_{outer} and σ_{inner} bands have sixfold modulations with angle φ, respectively, which are alternating with each other. This out-of-phase relation of σ_{outer} and σ_{inner} bands is consistent with observed band dispersions in Figs. 1(c) and 1(d). Such a strong intensity modulation provides an important clue to understanding the origin of kink
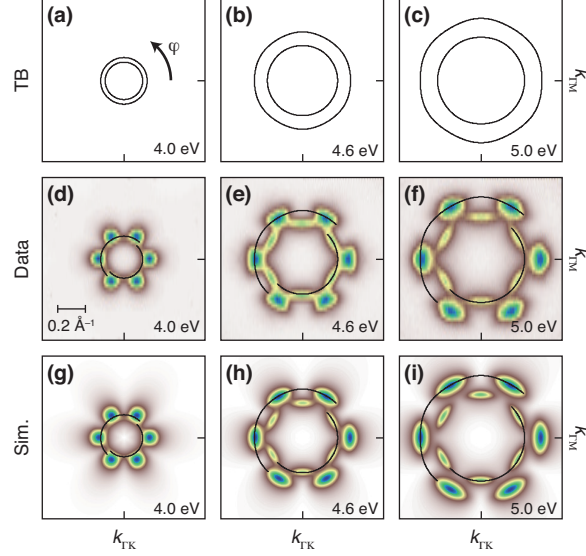
FIG. 2: (color online). (a)–(c) Constant-energy contours of tight-binding band calculations at binding energies marked at the bottom right. (d)–(f) Experimental ARPES intensity maps taken at corresponding binding energies with the photon energy of 36 eV. (g)–(i) Simulated ARPES intensity maps based on sublattice interference shown in Fig. 3. Overlaid lines are part of constant-energy contours shown in (a)–(c). The maximum intensity points in (d) and (g) slightly deviate from overlaid black lines due to the kink features.

features, as explained below.

ARPES intensity is subject to a strong modulation by the matrix element M^k that involves the quantum interference of wavefunctions. We have calculated M^k of σ bands based on the Fermi-Golden rule [32] that relates initial-state and final-state wavefunctions as,

$$M^k = \langle \psi_f^k \mid H_{int} \mid \psi_i^k \rangle = \sum_{n,l} A_l^k C_{l,n}^k e^{-ik \cdot \tau_n} F_l(k) \tag{1}$$

where A_l^k is the photoionization cross-section of orbital l with incident photons, $C_{l,n}^k$ is the coefficient of eigenvectors with momentum k and sublattice n, $F_l(k)$ is the Slater's orbital in k-space [34], τ_n is the distance of atomic basis in the form of plane waves [35]. The final state is approximated by a free electron based on the weak dependence of kink features on the photon energy [32]. This formula, which is also used to explain the spectral modulation in π bands of graphene and graphite [35–39], concerns the interference of photoelectrons coming from A and B sublattices of the honeycomb lattice (like two-source interference)
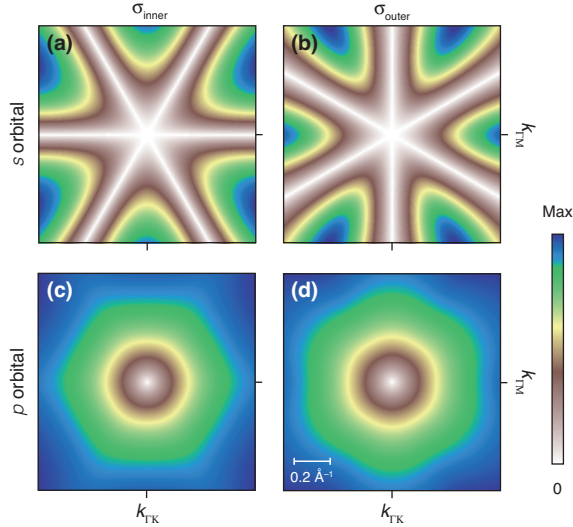
FIG. 3: (color online). The calculated interference-induced intensity maps for s and p orbitals of σ_{inner} and σ_{outer} bands, respectively, as marked at the top and the left. These maps are calculated based on the phase interference of initial-state wavefunctions coming from the two sublattices of graphene, as described in the text.

[36]. Here, we limit our analysis to the intrinsic phase interference of initial-state wavefunctions, and should be distinguished from final-state effects [38]. The details on initial-state wavefunctions, such as orbital amplitudes of A and B sublattices and their phase difference, are obtained from tight-binding calculations, as summarized in [32].

In Fig. 3, we display k distribution maps of sublattice interference calculated from the above formula for the s and p orbitals of σ_{inner} and σ_{outer} bands, respectively. The s orbital of σ_{inner} bands has the phase difference π along $k_{\Gamma K}$ [32], leading to destructive interference and resultant intensity pattern in the form of $\sin^2(6\varphi/2)$, as shown in Fig. 3(a). On the other hand, the phase difference along $k_{\Gamma K}$ is 0 for the s orbital of σ_{outer} bands, but their orbital amplitude vanishes along $k_{\Gamma M}$ [32]. The effect of constructive interference along $k_{\Gamma K}$ and amplitude suppression along $k_{\Gamma M}$ results in the intensity pattern in the form of $\cos^2(6\varphi/2)$, as shown in Fig. 3(b). The two sixfold intensity patterns of σ_{inner} and σ_{outer} bands, which are out of phase to each other [Figs. 3(a) and 3(b)], naturally explain our observations in Figs. 2(d)–2(f).

As for the p orbitals, the interference patterns of σ_{inner} and σ_{outer} bands commonly show much less anisotropy [Figs. 3(c) and 3(d)], as compared to those of s orbitals, suggesting
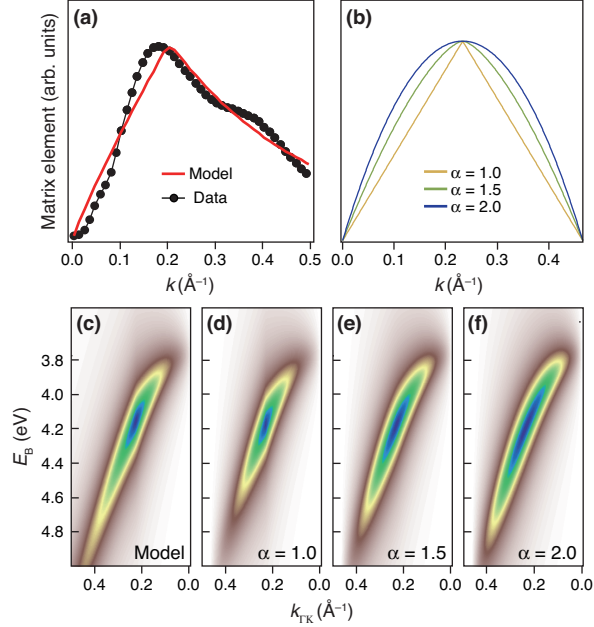
FIG. 4: (color online). (a) Matrix element as a function of k obtained by curve fitting to ARPES data in Fig. 1(c). The red line overlaid is used for model simulations in (c). (b) Matrix elements in the form of $1-|1-k/k_0|^\alpha$, where $k_0 = 0.23$ Å^{-1}. (c)–(f) A series of spectral simulations using matrix elements shown in (a) and (b) and marked at the bottom right.

that A_s is dominant over A_p in the photon energy of 30–45 eV. The ratio of A_s to A_p is also related to the linear polarization of photons and the scattering geometry in our experiments [40].

We have performed a simple spectral simulation with the standard Lorentzian formula [41] as

$$I(k, E) \propto \frac{\mathrm{Im}\Sigma(E)}{(E - E_{\mathrm{B}}(k))^2 + \mathrm{Im}\Sigma(E)^2} \cdot \left|M^k\right|^2 \tag{2}$$

where E_{B} is the band dispersion obtained from the tight-binding calculations for σ bands, and $\mathrm{Im}\Sigma(E)$ is the k independent imaginary part of self-energy. M^k is given by the above interference patterns, and A_s is reasonably assumed by reproducing experimental matrix elements [red curve in Fig. 4(a)]. $\mathrm{Im}\Sigma(E)$ is set by 50 meV at E_{F}, from which it monotonically increases with binding energy. This is to take into account finite broadening and the effect of electron correlation. On the other hand, electronic coupling to collective excitations is manifested by a step-like increase in $\mathrm{Im}\Sigma(E)$ at the energy scale of involved excitations [3–5], and is therefore not included in our simulations.

7

The resulting simulations are present in Figs. 2(g)–2(i) and Fig. 4(c), which successfully reproduce key aspects of our ARPES data, characteristic sixfold intensity patterns [Figs. 2(d)–2(f)] as well as strong intensity suppression near the Γ point [Fig. 1(c)]. More importantly, the kink features clearly appear in the simulated dispersion [Fig. 4(c)] without including the electron-phonon interaction [26]. This supports that the observed kink features are related to interference-induced intensity modulations rather than an intrinsic feature of the self-energy.

The strong intensity modulations in a narrow k region may lead to a kink feature, which has been debated in the study of high-energy kinks [9–16]. However, little is known about the origin of strong intensity modulations and really how such modulations result in a kink feature. In general, the matrix element M^k is a smoothly varying function within a single band. But in the presence of the sublattice (pseudospin) degree of freedom, the effect of phase interference may produce strong k dependence and resultant singular points in M^k. The abrupt variation of spectral intensity near a singular point makes k distribution curves slightly asymmetric. This causes a discrepancy in peak positions of energy and k distribution curves, leading to apparent kink features whose energy scale is simply set by the singular point and thus can be as high as few electronvolts.

This novel mechanism can be demonstrated by our simple but instructive model simulations shown in Figs. 4(d)–4(f). M^k is assumed to be a form of $1-|1-k/k_0|^\alpha$, where k_0 is the peak position and its curvature is parameterized by exponent α, as shown in Fig. 4(b). This is a minimal mathematical form of the red curve in Fig. 4(a) with the exponent α effectively controlling the degree of singularity at the k_0 point. The kink feature clearly appears for $\alpha = 1.0$ [Fig. 4(d)], which is in good agreement with Fig. 4(c). However, it becomes less pronounced for $\alpha = 1.5$ [Fig. 4(e)], and completely disappears at $\alpha = 2.0$ [Fig. 4(f)], where the singular point is absent in M^k [Fig. 4(b)]. Therefore, the formation of interference induced local singularity in M^k is a key factor that gives rise to the high-energy kink features in the σ bands of graphene. Our results establish the importance of the local singularity as a missing link between strong spectral modulations and high-energy kink features.

Our mechanism, which is demonstrated on graphene as a simple model system, works generally in the presence of a local singularity in M^k. Normally, M^k is a smoothly varying function within a single band, but a local singular point may be formed if there is strong phase interference. In fact, our explanation can also be extended to high-energy kinks or

waterfall dispersions observed in various transition-metal oxides, where the similar suppression of spectral intensity near the kink features was commonly observed [9–16]. Thus, the message of this work should be carefully considered in ARPES investigations to avoid any erroneous analysis.

It would also be interesting to discuss the effect of sublattice symmetry breaking on interference patterns. We found that the characteristic modulation of σ_{inner} bands [Fig. 3(a)] becomes progressively less anisotropic, as we increase the symmetry-breaking potential [32]. Our work thus suggests that strongly modulated intensity patterns measured by ARPES can be used to extract important physical information, such as quantum phases, (hidden) sublattices, and symmetry breaking.

––––––––

* keunsukim@postech.edu

[1] S. Hüfner, Photoelectron Spectroscopy (Springer, Berlin, 1995).

[2] A. Damascelli, Z. Hussain, and Z. -X. Shen, Rev. Mod. Phys. **75,** 473 (2003).

[3] T. Valla, A. V. Fedorov, P. D. Johnson, and S. L. Hulbert, Phys. Rev. Lett. **83,** 2085 (1999).

[4] A. A. Kordyuk, S. V. Borisenko, A. Koitzsch, J. Fink, M. Knupfer, and H. Berger, Phys. Rev. B **71,** 214513 (2005).

[5] K. Byczuk, M. Kollar, K. Held, Y. -F. Yang, I. A. Nekrasov, T. Pruschke, and D. Vollhardt, Nat. Phys. **3,** 168–171 (2007).

[6] A. Lanzara *et al.*, Nature **412,** 510–514 (2001).

[7] T. Valla, A. V. Fedorov, P. D. Johnson, B. O. Wells, S. L. Hulbert, Q. Li, G. D. Gu, and N. Koshizuka, Science **285,** 2110–2113 (1999).

[8] J. Schäfer, D. Schrupp, E. Rotenberg, K. Rossnagel, H. Koh, P. Blaha, and R. Claessen, Phys. Rev. Lett. **92,** 097205 (2004).

[9] J. Graf *et al.*, Phys. Rev. Lett. **98,** 067004 (2007).

[10] T. Valla, T. E. Kidd, W. -G. Yin, G. D. Gu, P. D. Johnson, Z. -H. Pan, and A. V. Fedorov,

Phys. Rev. Lett. **98,** 167003 (2007).

[11] D. S. Inosov *et al.*, Phys. Rev. Lett. **99,** 237002 (2007).

[12] W. Zhang *et al.*, Phys. Rev. Lett. **101,** 017002 (2008).

[13] S. Basak, T. Das, H. Lin, J. Nieminen, M. Lindroos, R. S. Markiewicz, and A. Bansil, Phys. Rev. B **80,** 214520 (2009).

[14] H. Iwasawa, Y. Yoshida, I. Hase, K. Shimada, H. Namatame, M. Taniguchi, and Y. Aiura, Phys. Rev. Lett. **109,** 066404 (2012).

[15] E. D. L. Rienks, M. Ärrälä, M. Lindroos, F. Roth, W. Tabis, G. Yu, M. Greven, and J. Fink, Phys. Rev. Lett. **113,** 137001 (2014).

[16] Y. Liu *et al.*, Sci. Rep. **75,** 13036 (2015).

[17] A. Bostwick, T. Ohta, T. Seyller, K. Horn, and E. Rotenberg, Nat. Phys. **3,** 36–40 (2007).

[18] S. Y. Zhou, D. A. Siegel, A. V. Fedorov, and A. Lanzara, Phys. Rev. B **78,** 193404 (2008).

[19] A. Bostwick, F. Speck, T. Seyller, K. Horn, M. Polini, R. Asgari, A. H. MacDonald, and E. Rotenberg, Science **328,** 999–1002 (2010).

[20] D. A. Siegel, C. -H. Park, C. Hwang, J. Deslippe, A. V. Fedorov, S. G. Louie, and A. Lanzara, Proc. Natl. Acad. Sci. U.S.A. **108,** 11365 (2011).

[21] M. Calandra and F. Mauri, Phys. Rev. Lett. **95,** 237002 (2005).

[22] M. Calandra and F. Mauri, Phys. Rev. B. **76,** 205411 (2007).

[23] W. -K. Tse and S. Das Sarma, Phys. Rev. Lett. **99,** 236802 (2007).

[24] C. -H. Park, F. Giustino, M. L. Cohen, and S. G. Louie, Nano Lett. **8,** 4229–4233 (2008).

[25] C. -H. Park, F. Giustino, J. L. McChesney, A. Bostwick, T. Ohta, E. Rotenberg, M. L. Cohen, and S. G. Louie, Phys. Rev. B **77,** 113410 (2008).

[26] F. Mazzola *et al.*, Phys. Rev. Lett. **111,** 216806 (2013).

[27] K. V. Emtsev *et al.*, Nat. Mater. **8,** 203–207 (2009).

[28] C. Riedl, C. Coletti, T. Iwasaki, A. A. Zakharov, and U. Starke, Phys. Rev. Lett. **103,** 246804 (2009).

[29] F. Speck, J. Jobst, F. Fromm, M. Ostler, D. Waldmann, M. Hundhausen, H. B. Weber, and T. Seyller, Appl. Phys. Lett. **99,** 122106 (2011).

[30] S. Konschuh, M. Gmitra, and J. Fabian, Phys. Rev. B **82,** 245412 (2010).

[31] M. Hollering, J. Bernhardt, J. Schardt, A. Ziegler, R. Graupner, B. Mattern, A. P. J. Stampfl, U. Starke, K. Heinz, and L. Ley, Phys. Rev. B **58,** 4992 (1998).

[32] See supplementary materials at http://link.aps.org/supplemental/ for additional figures on the details of sublattice-interference calculations and the photon-energy dependence of ARPES data.

[33] J. Sforzini *et al.,* Phys. Rev. Lett. **114,** 106804 (2015).

[34] D. Belkić, and H. S. Taylor, Phys. Scr. **39,** 226 (1989).

[35] E. L. Shirley, L. J. Terminello, A. Santoni, and F. J. Himpsel, Phys. Rev. B **51,** 13614 (1995).

[36] M. Mucha-Kruczyński, O. Tsyplyatyev, A. Grishin, E. McCann, V. I. Fal'ko, A. Bostwick, and E. Rotenberg, Phys. Rev. B **77,** 195403 (2008).

[37] Y. Liu, G. Bian, T. Miller, and T. -C. Chiang, Phys. Rev. Lett. **107,** 166803 (2011).

[38] I. Gierz, J. Henk, H. Höchst, C. R. Ast, and K. Kern, Phys. Rev. B **83,** 121408(R) (2011).

[39] C. Hwang, C. -H. Park, D. A. Siegel, A. V. Fedorov, S. G. Louie, and A. Lanzara, Phys. Rev. B **84,** 125422 (2011).

[40] L. Moreschini *et al.,* Phys. Rev. Lett. **112,** 087602 (2014).

[41] K. S. Kim, A. L. Walter, L. Moreschini, T. Seyller, K. Horn, E. Rotenberg, and A. Bostwick, Nat. Mater. **12,** 887–892 (2013).